PCCP

Accepted Manuscript

ROYAL SOCIETY OF CHEMISTRY

www.rsc.org/pccp

Direct Imaging of Layered O3- and P2-$Na_xFe_{1/2}Mn_{1/2}O_2$ Structures at Atomic Scale

Xia Lu[1, 2], Yuesheng Wang[1], Pin Liu[1], Lin Gu[1,*], Yong-Sheng Hu[1,*], Hong Li[1], George P. Demopoulos[2] and Liquan Chen[1]

1. *Beijing National Laboratory for Condensed Matter Physics, Institute of Physics, Chinese Academy of Sciences, Beijing, 100190, China.*
2. *Department of Materials Engineering, McGill University, 3160 University Street, Montréal (Québec), Canada, H3A 0C5.*

Corresponding author: yshu@aphy.iphy.ac.cn; l.gu@iphy.ac.cn

Abstract: Using aberration-corrected scanning transmission electron microscopy (STEM) with high-angle annular-dark-field (HAADF) and annular-bright-field (ABF) techniques, the atomic-scale structures of the O3 and P2 phases $Na_xFe_{1/2}Mn_{1/2}O_2$ are investigated systematically. The Na, transition metals **M** (Fe and Mn) and O columns are well revealed and precisely assigned to the O3 and P2 phase layered structures. The O3 phase sample demonstrates the larger atomic site fluctuations along [001] direction but with less structure imperfections (*e.g.* interlayer structure and stacking defaults) than in the P2 phase sample. Furthermore, a clear surface with regular structure is observed for O3- $NaFe_{1/2}Mn_{1/2}O_2$ sample while a surface with a large amount of ***Na*-M** antisites is observed for P2-$Na_{2/3}Fe_{1/2}Mn_{1/2}O_2$ sample.

Keywords: $Na_xFe_{1/2}Mn_{1/2}O_2$; P2 phase; O3 phase; Atomic structure; Scanning transmission electron microscopy.

1. Introduction

Long-life sodium-ion battery, which has been regarded as promising electrochemical means to store electrical energy in large-scale, is a hot topic and an important direction in this field. Although many materials have been proposed[1-22], the sodium storage mechanisms and the relationship between the structure evolutions and the electrochemical performance are far from well understood. In order to speed up the exploration of new and better materials, the in-depth understanding of this electrode material relationship is quite critial for sodium-ion batteries. Among the avaliable structures, the layer-structured materials $\boldsymbol{A}\mathbf{M}O_2$ (***A*** = Li, Na; **M** = transition metals) are particularly promsing candidates for Li/Na ion cathodes. Comparing Li and Na materials, the O3 phase is the easily available structure for $\boldsymbol{Li}\mathbf{M}O_2$, while in the case of $\boldsymbol{Na}_x\mathbf{M}O_2$ ($2/3 \leq \boldsymbol{x} \leq 1.0$) is the O3 and/or P2 phases. Crystallographically, the ***A*** ions locate between two **M**-O octahedron slabs along [001] direction and they reside at the octahedral sites (O_h coordination) in O3 structrue and at the prismatic sites (D_{3h} coordination) in P2 structure respectively. Based on the atomic arrangement of oxygen layers, the $\boldsymbol{A}\mathbf{M}O_2$ structures can be assigned to the O3, O1, P2, O2 and P3 phases, *etc.*[23, 24]. Figure 1 illustrates the O3 and P2 atomic structures of the layered $\boldsymbol{A}\mathbf{M}O_2$ viewed from [010] direction. From Figure 1, the O columns stack in a ABCABC- mode and the **M** ion follows the αβγ-stacking mode in O3 phase; at the same time the O columns display the ABBA-stacking mode and only one **M** ion site in AAA-stacking mode in the P2 structure along [001] direction. Concerning the ***A*** ion occupations, it only takes the crystallographical *3b* site as regular $\boldsymbol{A}O_6$ octahedra with edge-shared connection with $\mathbf{M}O_6$ octahedra in the O3 phase; while the ***A*** ions fractionally occupy the *2b* and *2d* sites as $\boldsymbol{A}O_6$ prisms in P2 structure with some evident distortions. In P2 structure as shown in Figure 1b, two different ***A*** ion sites demonstrate a zig-zag distribution along [010] direction. The *2b* site $\boldsymbol{Na}O_6$ octahedron exhibits edge-sharing, while the *2d* site $\boldsymbol{Na}O_6$ octahedron exhibits face-sharing with the $\mathbf{M}O_6$ octahedra; in the meantime the *2d* Na ion

resides on a less stable structure site than the *2b* site[25]. The ***A***-O octahedra/prisms share the edges and/or faces with $\mathbf{M}O_6$ octahedra and the empty tetrahedral sites distribute uniformly among them, which is important for the evolution of the stucture upon ***A*** insertion/extraction and also for ***A*** ion diffusion through the host structure[26].

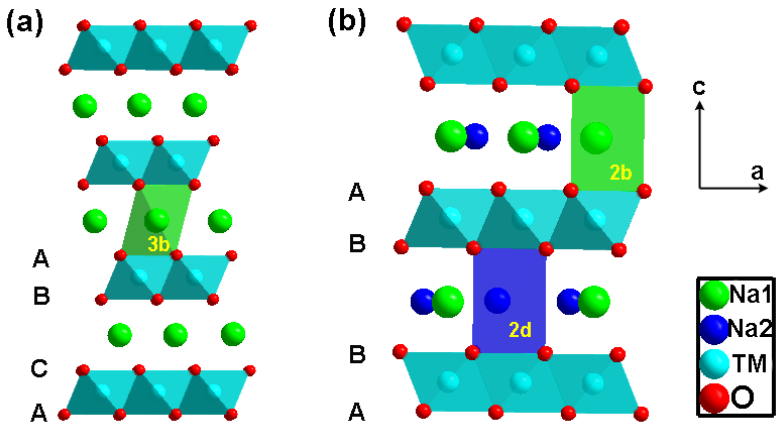

Figure 1. Schematic illustrations of the O3 and P2 structures at [010] direction. (a) The oxygen columns demonstrate the ABCABC-stacking model and the **M** ions display the αβγ-stacking model in O3 phase; (b) the oxygen columns give the ABBA-stacking model and the **M** ions exhibit the ααα-stacking model in P2 phase. The ***Na*** ions only occupy the *3b* site in the O3 phase, while fractionally take the *2b* and *2d* sites in the P2 structure. Crystallographically, the Li/Na ions locate between two **M**-O octahedron slabs along [001] direction.

As to the Na ion storage and transport mechanism (electrochemistry - structure relatuonship) in this layered materials, it can date back to the 1980s for sodium ion battery[27-29]. In the early work, Delmas, C. *et al.* reported phase transitions in the electrochemically active O3-$NaCoO_2$, P'3-$Na_{0.66}CoO_{1.92}$, O'3-$Na_{0.77}CoO_{1.92}$ and P2-$Na_{0.70}CoO_{1.96}$ phases during desodiation/sodiation[28]. They revealed by XRD analysis that the P2 structure is maintained over the whole composition range $0.46 \leq x \leq 0.83$[28]. Then Molenda, J. *et al.* demonstrated the initial concentration of electronic carriers to be a Na-dependent insertion property in the case of P2-$Na_{0.70}CoO_{2-y}$ cathode[30]. After that, Viciu, L. *et al.* reported several complex Na content–dependent sructure in Na_xCoO_2 with x = 0.32, 0.51, 0.60, 0.75 and 0.92 as determined by powder neutron diffraction and they revealed that the underlying CoO_2 lattice experiences some kind of structural modulation at

x = 0.75 composition[31]. Shu, J. G. *et al.* investigated the Na^+ ion diffusion and ordering properties in a P2-Na_xCoO_2 single crystal using the PITT technique. They demonstrated that excluding the significantly slower diffusion behavior near particular Na ordered phases, the average diffusion coefficients D_{Na} to be 10^{-7} cm^2/s for x > 0.5 and 10^{-8} cm^2/s for x < 0.5, respectively[32]. Subsequently, Berthelot, P. *et al.* systematically investigated the P2-Na_xCoO_2 phase diagram and identified at room temperature nine single-phase domains with narrow sodium composition ranges due to peculiar Na^+/Na vacancy ordering[25]. Very recently, Yabuuchi, N. *et al.* reported that the P2-$Na_{2/3}Fe_{1/2}Mn_{1/2}O_2$ phase delivers 190 mAh/g of reversible capacity with the electrochemically active Fe^{3+}/Fe^{4+} redox couple, much higher than the 110 mAh/g reversible capacity for O3-$Na_{2/3}Fe_{1/2}Mn_{1/2}O_2$ phase, showing promising potential applications[14]. Consequently, it can be summarized that the layered $\boldsymbol{Na_xMO_2}$ materials are structure-dependent cathodes with complex phase transitions during desodiation/sodiation and lots of studies are in need to be further devoted to clarifying the structure of this layered materials for sodium-ion batteries.

In terms of electrochemical performance, a solid-solution reaction with (a) an initial short-plateau region and (b) a subsequent long slope region[33] is always observed in O3-$\boldsymbol{LiMO_2}$ (**M** = Co) cathode for Li-ion battery. However, there are a series of plateaus appearing on the charge/discharge curves of the P2-$\boldsymbol{Na_xMO_2}$ (**M** = Co) cathode for Na-ion battery[13, 14]. Moreover the structure stabilities of $\boldsymbol{AMO_2}$ cathodes, including the structure evolutions, ***A***-**M** antisites, phase transitions and the charge compensation from the oxygen matrix are still under dispute. Therefore it is necessary to get detailed structural information, which is benificial for dealing with such encountered issues. In this work, the layered O3/P2-$\boldsymbol{Na_x}Fe_{0.5}Mn_{0.5}O_2$ samples are synthesized and the related atomic structures are carefully investigated using spherical aberration-corrected scanning transmission electron microscopy (STEM) with high-angle annular-dark-field (HAADF) and annular-bright-field (ABF) techniques.

2. Experimental section

The $\boldsymbol{Na}_x Fe_{0.5}Mn_{0.5}O_2$ samples were synthesized *via* a solid-state reaction according to the references[14, 25]. In a typical synthetic process, the stoichiometric amounts of sodium peroxide (Na_2O_2), iron oxide (Fe_2O_3) and manganese(III) oxide (Mn_2O_3) powders were mixed and grounded adequately in golve box. Then the mixed powder was pelleted into slices. The slices were heated at 700^0C, 36h for O3 phase and 900^0C, 12h for P2 phase at the heating rate of 5^0C/min in the muffle furnace. After the temperature was cooled naturally down to room temperature, the O3-/P2- $\boldsymbol{Na}_x Fe_{0.5}Mn_{0.5}O_2$ samples were obtained.

X-ray powder diffraction (XRD) patterns were collected in the range of 10 – 80 ° using a Philips X'pert diffractometer with Bragg-Brentano geometry. The measurement was performed in a continuous scan mode, using Cu Kα X-ray source and a step of 0.0167 °/s. A scanning electron microscope (SEM) (Hitachi S-4800) was used to study the morphology. Aberration-corrected scanning transmission electron microscopy was performed using a JEOL 2100F (JEOL, Tokyo, Japan) transmission electron microscope equipped with a CEOS (CEOS, Heidelberg, Germany) probe aberration corrector. The attainable spatial resolution of the microscope is 90 picometer at an incident angle of 40 mrad.

3. Results and discussion

The P2 and O3 type materials are two main groups for sodium-based layered electrodes. Figure 2 shows the XRD patterns and the SEM morphologies of the as-prepared P2 and O3 layered samples. From the Figure 2a, the XRD patterns can be well indexed to the P2 type and O3 type $\boldsymbol{Na}_x Fe_{0.5}Mn_{0.5}O_2$ samples (hereafter denoted as P2-NaFMO and O3-NaFMO) with minor impurities. The impurities are always indicative of the formation of other types of layer-structured materials and/or metal oxides during synthesis[14, 25]. From the SEM micrographs, the P2-NaFMO samples have larger particle size than that of the O3-NaFMO samples on average and the primary particles agglomerate together to form big secondary particles. Concerning the electrochemical performance, Yabuuchi, *et al*. reported

that the P2-NaFMO electrode delivered about 190 mAh/g in the voltage range of 1.5 - 4.2 V, which is higher than 110 mAh/g delivered by the O3-NaFMO sample as cathode in half cells[14]. Furthermore, they found the P2-OP4 phase transition upon desodiation in P2-NaFMO electrode and O3-P3-OP2 phase transition upon desodiation in O3-NaFMO electrode using synchrotron X-ray diffraction method[14]. These phase transitions are caused probably by the interaction of the Na^+ ion vacancies with the transition metal octahedra, which are the common phenomena in layered materials for rechargeable batteries[33-36].

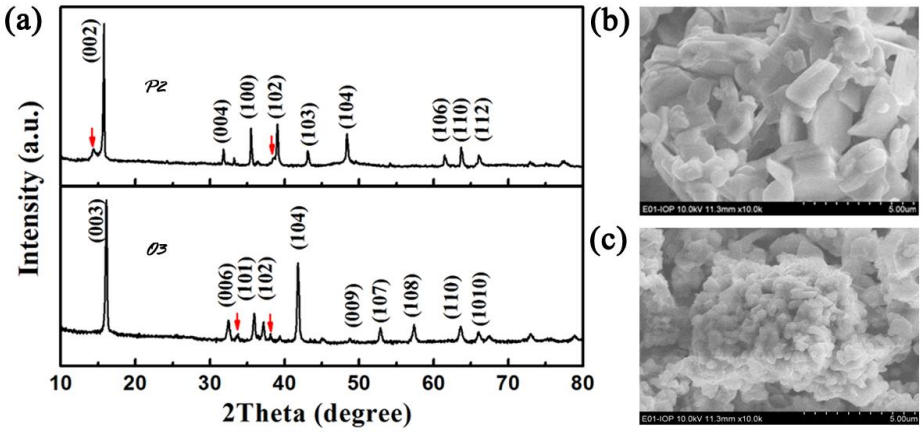

Figure 2. XRD patterns and SEM images for (a) & (b) layered P2-phase $Na_{2/3}Fe_{1/2}Mn_{1/2}O_2$ and (a) & (c) O3-phase $NaFe_{1/2}Mn_{1/2}O_2$ samples. Most peaks can be exactly indexed to the P2 and O3 $Na_xFe_{1/2}Mn_{1/2}O_2$ phases, respectively. In addition, the red arrows demonstrate the minor impurities in the as-prepared samples, which are difficult to eliminate during synthetic process.

From the viewpoint of structure stability, the layered battery materials are apt to adjust their energetically favorable configuration when *x* changes in $\boldsymbol{A_xMO_2}$ structure and after that it tries to maintain the corresponding states. Therefore for a perfect layered crystal, the stucture varies with the *x* value, *i.e.* phase transitions (or structure evolutions) happen accordinglly. In order to elucidate these phase variations, structure characterizations are executed on $\boldsymbol{Na_x}Fe_{0.5}Mn_{0.5}O_2$ samples using aberration-corrected STEM with high-angle annular-dark-field (HAADF) and annular-bright-field (ABF) techniques. STEM techniques have proven very successful in rechargeable battery research as they allow for precise atomic positions (such as light element Li, O), structure defects, phase evolution and phase/grain boundaries to be clearly acquired at atomic scale[33, 37-43], hence advancing the deeper comprehension

on ion storage and transport. It is worth of mentioning that the contrast of the HAADF image follows a $Z^{1.7}$ dependence as compared with $Z^{1/3}$ for ABF the image with respect to the atomic number (Z)[41, 44, 45].

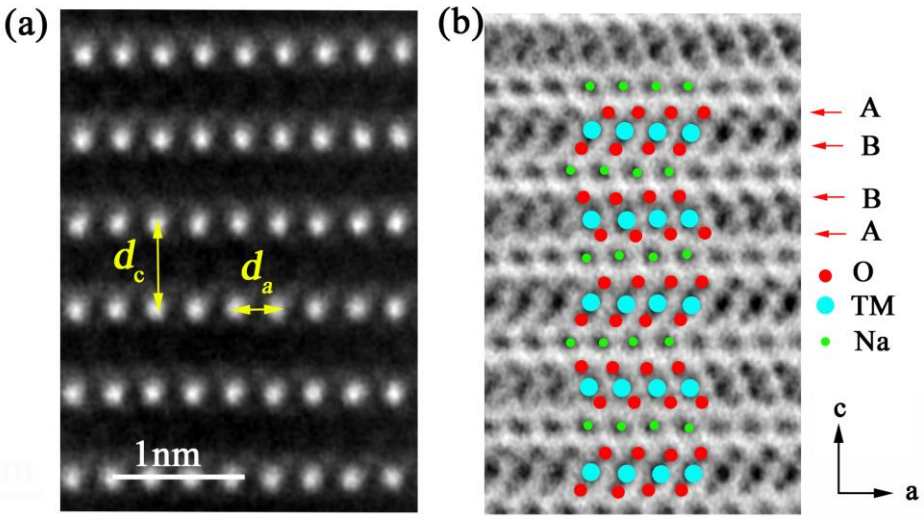

Figure 3. STEM (a) HAADF and (b) ABF images for the as-prepared P2-phase $Na_{2/3}Fe_{1/2}Mn_{1/2}O_2$ materials at [010] zone axis. The d_c and d_a represent the distance of (003) plane and the distance of two **M** columns along [010] direction. The original pictures are presented in the supporting Figure S1.

Figures 3 and S1 demonstrate the filtered STEM HAADF and ABF images of P2-NaFMO sample. From Figure 3a of the HAADF image, it reveals the ordered arrangement of the transition metal **M** (Fe and Mn) columns at [010] zone axis. Along either [100] or [001] direction, the **M** columns align straightforwardly, which is totally different form the O3-NaFMO samples as discussed later. The distance of the adjacent layer d_c is *ca.* 0.60 nm, is a little larger than the reported 0.56 nm value[14], which is probably caused by nano-sizing effects and/or the different synthesis conditions employed. Moreover, from the ABF image in Figure 3b, the light element ***Na*** and O columns can be distinguishably identified besides the **M** columns, which are also shown in Figure S1d. The ***Na***, O and **M** columns have also different contrasts in the ABF image as shown in Figure S1d. For the **M** columns, a ααα-stacking mode is shown, the same as that in Figure 3a; for the O columns, a distinct ABBA-stacking mode is shown at the acquired ABF picture. Each O column follows the same stacking mode as one of the adjacent O columns but with a site shift (0.5 d_a) to the other adjacent O column along [001] direction, displaying a mirroring symmetry,

when referred to the Na ion layer at [010] zone axis; for ***Na*** columns, it demonstrates a regular ABAB-stacking mode along [001] direction. Note that the Na1 and Na2 columns are too close to be distinguishable and their contrasts overlap with each other as one column to a great extent when projected along [100] direction as shown in Figure 3b and Figure S1e. One ***Na***O_6 prism is employed as a medium to connect two **M**O_6 octahedra and minimize the coulombic repulsion interaction hence stabilizing the P2 layered structure.

However in P2-layered structures, it is difficult to get samples with Na ions fully occupying the octahedra/prisms in (003) face, which means it is hard to obtain the stoichiometric formula ***Na*****M**O_2. If the two Na ions approach closer like the Li-Li distance in O3-$LiCoO_2$ structure, the Na ion will repel the adjacent one to create Na vacancies due to a larger ***Na*** ion radius. Therefore here in Figure 3b the ***Na*** ion columns are fractionally filled to leave a certain amount of Na vacancies in the as-prepared samples. Furthermore the Na vacancies show no evidence of clustering or ordering arrangements based on the small contrast changes of each Na column along [100] direction (refer to Figure S1e). In addition, a certain amount of Na vacancies in the structure are beneficial for: 1) structure stability and 2) Na^+ ion transport.

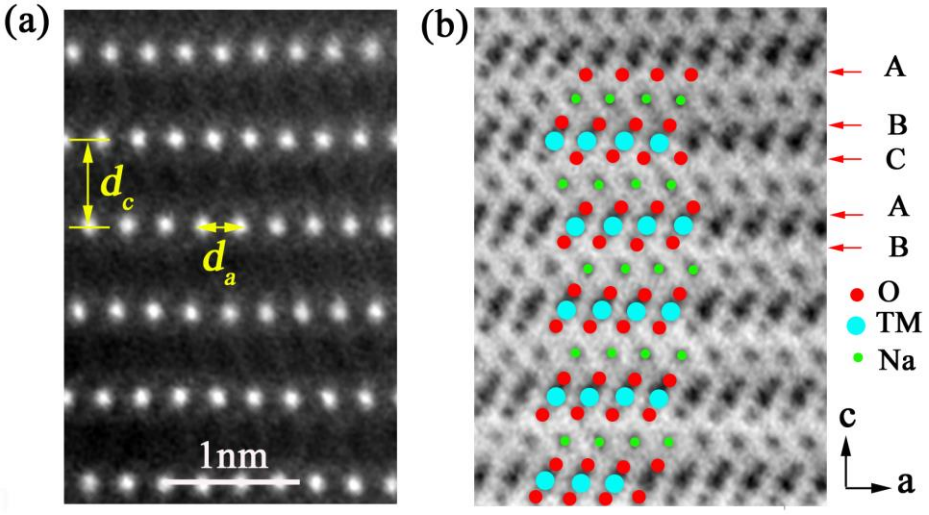

Figure 4. STEM (a) HAADF and (b) ABF images for the as-prepared O3-phase $NaFe_{1/2}Mn_{1/2}O_2$ sample at [010] zone axis. The d_c and d_a represent the distance of (003) plane and the distance of two **M** columns along [010] direction. The original pictures are presented in the supporting Figures S2.

The O3-NaFMO sample unfolds a different physical picture from that of

P2-NaFMO sample as shown in Figure 4. From Figure 4a of the HAADF image, the **M** columns align in line along [100] direction, the same as in the P2-NaFMO HAADF image. However along [001] direction, each **M** column shows a site glide of the 2/3 d_a, when compared with the adjacent layers. Therefore every three other layer we have the same **M** column occupations and the **M** column duplicates the ABCABC-stacking mode to form the O3 structure along [001] direction. Likewise, the distance of adjacent layer d_c is *ca.* 0.61 nm, still a little larger than the reported value of 0.55 nm[14]. From Figure 4b of the ABF image and Figure S2c, it demonstrates the unambiguous contrast of ***Na***, **M** and O columns. All of the three different columns take the same ABCABC-stacking mode in the atomic arrangements. However, there is a little difference for the O columns. As shown in Figure 4b, the layer distance of each O column shows much different from the head-to-head stacking (ABBA) mode of P2 phase in Figure 3b along [001] direction. Apparently upon ion extraction/insertion, the O matrix is easier to glide in the P2 structure than that in the O3 structure, because the O3 structure is the thermodynamically equilibrated configuration based on theoretical calculations[33]. However structure changes still happen irreversibly, when the alkali metal ***A*** vacancies accumulate to some extent in both structures[14]. The structure relaxes into new configurations from which it is hard to recover back into the initial structure due to eventual introduction of vacancies upon alkali metal ***A*** extraction.

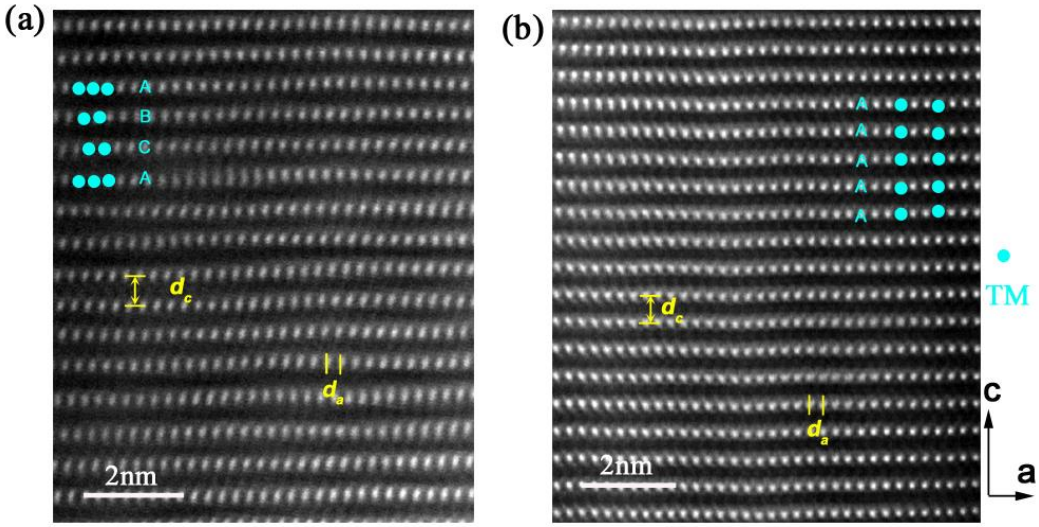

Figure 5. STEM HAADF images for (a) O3-phase $NaFe_{1/2}Mn_{1/2}O_2$ sample and (b) P2-phase $Na_{2/3}Fe_{1/2}Mn_{1/2}O_2$ sample at [010] zone axis. The d_c and d_a represent the distance of (003) plane and the distance of two **M** columns along [010] direction. The original pictures are presented in

the supporting Figures S3.

In the small regions of the HAADF and ABF images (see Figure 3 and Figure 4), P2 and O3 layered structures are shown with nearly ideal Na, O and **M** atomic arrangements. However, structure distortions and defects are always present in these ordered structures as demonstrated in Figure 5 and Figure S3. Actually these structure imperfections apparently play an important role in ion storage and transport. From the HAADF image of Figure 5a and Figure S3a, it reveals the remarkable structure distortion in the O3-NaFMO sample. From the [100] direction, the **M** site fluctuations cause the variations of the (003) planar distance. The d_c is estimated to be 0.61 ± 0.10 nm. Due to negligible Na^+ ion vacancies, the Na-Na distance decreases in (003) plane, which in turn causes strong Na^+-Na^+ repulsion introducing larger distortion in the ***Na***O_6 octahedron that is ultimately responsible for the observed layer distance fluctuations in O3 structure[33]. Crystallographically, the layer distance is far larger than the diameter of Na^+ ion (~ 0.20 nm); therefore it should be beneficial for Na storage and diffusion. However, the distortion induced by the Na^+ ion vacancies is believed to set several changes in motion: 1) macroscopically, the ***Na***, **M** and O arrays are displaced to find a new thermodynamically equilibrated configuration that has as consequence reaching a new stable phase with a new chemical potential μ modifying the cell voltage accordingly; 2) microscopically, the Na ion O_h symmetry is broken causing lattice field interruption and the introduction of coulombic interaction between the two **M**O_6 slabs. That is, the created Na^+ ion vacancies contribute a lot to structure instability. Furthermore by observing Figure S3a, some local microstructure with other **M** stacking mode can be seen, such as O2-like microstructures (**M** in αβ-stacking and O in ABAC-stacking, see Figure S5), which are directly related with this local layer structure change/distortion.

For the O3-NaFMO sample, the most observed phenomenon is the remarkable layer distortions, while for P2-NaFMO sample, more information can be acquired from the HAADF images as shown in Figure 5b and S3b~3e. In Figure 5b, the layer distance was measured to be 0.60 ± 0.04 nm with the layer stripe clearly shown along

[100] direction. The fluctuation of layer distance seems smaller than that of the O3-NaFeMO sample along [001] direction. However, the structure imperfections increase significantly. Firstly in the yellow arrow region of Figure S3b ~ 3e, it can be observed that there are some unexpectedly larger layer distances, which are nearly twice of the regular d_c value. This kind of layer expansion seems plausibly beneficial for Na^+ ion diffusion. Furthermore in Figure S3b, it also demonstrates the layer stacking default, which gives birth to a *ca.* 5^o angle as shown in the green and yellow line parts. This can be treated as the interface of two particles, which will merge together to form a new bigger particle. In Figure S3c, a few intercalated layers are witnessed in the bulk of one particle, which are probably caused by ***Na*-M** antisites formed during annealing. Here, the adjacent coordination of Na^+ ion changes from only the O ions to the O and **M** ions, which should play an important role in the evolution of structure and even battery failure upon sodiation/de-sodiation. The intercalated structures are also found in the surface region of the P2-NaFMO sample, which extends from the outmost surface to the bulk, about 20 nm far away from the surface as shown in Figure S3d.

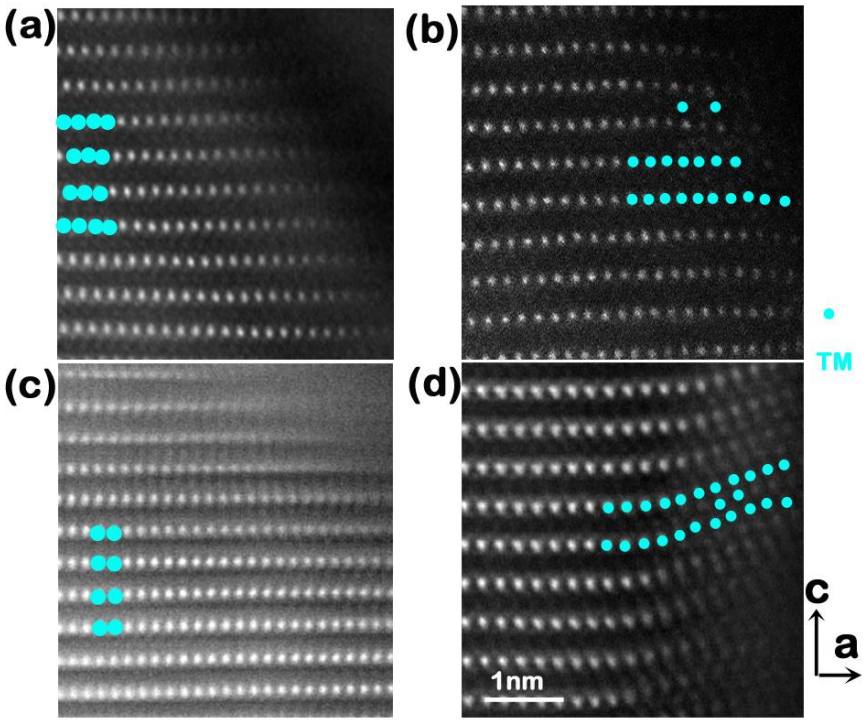

Figure 6. STEM HAADF images of the surface structures without (a) and with (b) a few ***Na*-M**

antisites for the as-prepared O3-phase $NaFe_{1/2}Mn_{1/2}O_2$; surface structures without (c) and with (d) obvious ***Na*-M** antisites for the as-prepared P2-phase $Na_{2/3}Fe_{1/2}Mn_{1/2}O_2$ at [010] zone axis. The original pictures are presented in the supporting Figure S4.

The O3-NaFMO particles display larger ***Na***, **M** and O site fluctuations along [001] direction than in the case of the P2-NaFMO particles. Thus concerning surface structures as shown in Figure 6, the O3-NaFMO sample demonstrates remarkably different structure with that of the P2-NaFMO sample. From Figure 6a and Figure S4a ~ S4b, the HAADF image of the O3-NaFMO sample is seen to exhibit ordered **M** columns aligned straightforwardly from the bulk to the surface, so do the ***Na*** and O columns along [100] direction (ABF image in Figure S4c). This gives a clear O3-NaFMO surface structure. However, a local region with negligible ***Na*-M** antisites was observed in Figure 6b and Figure S4d, which are likely introduced by surface relaxation to excite the ***Na*** ions interchanging with **M** ions. Therefore the **M** columns do not strictly follow the αβγ-stacking fault (Figure S5a and S6a) but have slightly disordered arrangements in several surface layers along [001] direction. In contrast, this disordered stacking mode seems to facilitate the formation of ***Na*-M** antisites in the surface region after cycling[33]. In Figure 6c and 6d, the HAADF images reveal the surface structure without/with ***Na*-M** antisites in P2-NaFMO sample. A typical difference is that the amount of ***Na*-M** antisites increases to a great extent and can be easily found in the available surface region when compared with that in O3-NaFMO surface. In the enlarged HAADF image of Figure S4f, a large area with fully ***Na*-M** antisites was found to cover the surface of the P2-NaFMO sample. This can also be confirmed by the enhanced contrast of the Na columns in ABF image of Figure S4g. Therefore it shows that a clear surface is easily formed in the case of the O3-NaFMO sample, while in the case of P2-NaFMO sample a surface with significant ***Na*-M** antisites forms instead.

4. Conclusions

O3 and P2 phase $Na_xFe_{1/2}Mn_{1/2}O_2$ samples were synthesized by a solid state method and investigated using aberration-corrected scanning transmission electron microscopy (STEM) with high-angle annular-dark-field (HAADF) and

annular-bright-field (ABF) techniques. The XRD patterns of the as-prepared samples can be well indexed to the O3 and P2 phases although some minor impurities were present. The HAADF and ABF images were acquired with clear ***Na***, **M** (Fe and Mn) and O occupations at atomic scale. Some new insights concerning the structure and phase transitions during sodiation/de-sodiation are achieved:

For the O3 phase, the O columns follow the ABCABC-stacking mode in the ABF image. The O3 structure demonstrates obvious site fluctuation with the layer distance $d_c \sim 0.61 \pm 0.10$ nm along [001] direction in the HAADF image. Furthermore, a clear and ordered atomic arrangement was observed with negligible ***Na***-**M** antisites in several outmost surface layers.

For the P2 phase, it was unambiguously observed to have regular ***Na*** and O in ABBA-stacking, **M** in ααα-stacking modes along [001] direction. The P2 phase also demonstrates a regular layer distance with fewer fluctuations. Moreover, some obvious structure imperfections are detected accordingly from the HAADF and ABF images, including the stacking faults, intercalated structure and remarkable layer distortion. Comparing with the O3 sample, the P2 phase $Na_{2/3}Fe_{1/2}Mn_{1/2}O_2$ sample demonstrates a surface structure with a large amount of ***Na***-**M** antisites.

Acknowledgements

This work was supported by funding from the "973" Projects (2010CB833102, 2012CB932900), NSFC (51222210, 11234013, 11174334), "Strategic Priority Research Program" of the Chinese Academy of Sciences (Grant No. XDA01020304) and One Hundred Talent Project of the Chinese Academy of Sciences.

References:

1. Pan, H. L.; Hu, Y. S.; Chen, L. Q., Room-temperature stationary sodium-ion batteries for large-scale electric energy storage. *Energ Environ Sci* **2013,** 6, (8), 2338-2360.
2. Kim, S. W.; Seo, D. H.; Ma, X. H.; Ceder, G.; Kang, K., Electrode Materials for Rechargeable Sodium-Ion Batteries: Potential Alternatives to Current Lithium-Ion Batteries. *Adv Energy Mater* **2012,** 2, (7), 710-721.
3. Slater, M. D.; Kim, D.; Lee, E.; S., J. C., Sodium-Ion Batteries. *Adv. Funct. Mater.* **2012**, (23), 947.
4. Palomares, V; Casas-Cabanas, M; Castillo-Mart ńez, E.; Man H. Hanb, M. H.; Rojo, T.; Update on Na-based battery materials. A growing research path. *Energy Environ. Sci.*, **2013**, 6 , 2312-2337.
5. Komaba, S.; Murata, W.; Ishikawa, T.; Yabuuchi, N.; Ozeki, T.; Nakayama, T.; Ogata, A.; Gotoh, K.; Fujiwara, K., Electrochemical Na Insertion and Solid Electrolyte Interphase for Hard-Carbon Electrodes and Application to Na-Ion Batteries. *Adv Funct Mater* **2011,** 21, (20), 3859-3867.
6. Park, Y. U.; Seo, D. H.; Kwon, H. S.; Kim, B.; Kim, J.; Kim, H.; Kim, I.; Yoo, H. I.; Kang, K., A New High-Energy Cathode for a Na-Ion Battery with Ultrahigh Stability. *J Am Chem Soc* **2013,** 135, (37), 13870-13878.
7. Kim, D.; Lee, E.; Slater, M.; Lu, W. Q.; Rood, S.; Johnson, C. S., Layered Na[Ni1/3Fe1/3Mn1/3]O-2 cathodes for Na-ion battery application. *Electrochem Commun* **2012,** 18, 66-69.
8. Zhao, J. M.; Jian, Z. L.; Ma, J.; Wang, F. C.; Hu, Y. S.; Chen, W.; Chen, L. Q.; Liu, H. Z.; Dai, S., Monodisperse Iron Phosphate Nanospheres: Preparation and Application in Energy Storage. *Chemsuschem* **2012,** 5, (8), 1495-1500.
9. Pan, H. L.; Lu, X.; Yu, X. Q.; Hu, Y. S.; Li, H.; Yang, X. Q.; Chen, L. Q., Sodium Storage and Transport Properties in Layered Na2Ti3O7 for Room-Temperature Sodium-Ion Batteries. *Adv Energy Mater* **2013,** 3, (9), 1186-1194.
10. Hosono, E.; Saito, T.; Hoshino, J.; Okubo, M.; Saito, Y.; Nishio-Hamane, D.; Kudo, T.; Zhou, H. S., High power Na-ion rechargeable battery with single-crystalline Na0.44MnO2 nanowire electrode. *J Power Sources* **2012,** 217, 43-46.
11. Komaba, S.; Yabuuchi, N.; Nakayama, T.; Ogata, A.; Ishikawa, T.; Nakai, I., Study on the Reversible Electrode Reaction of Na1-xNi0.5Mn0.5O2 for a Rechargeable Sodium-Ion Battery. *Inorg Chem* **2012,** 51, (11), 6211-6220.
12. Liu, Y. L.; Xu, Y. H.; Han, X. G.; Pellegrinelli, C.; Zhu, Y. J.; Zhu, H. L.; Wan, J. Y.; Chung, A. C.; Vaaland, O.; Wang, C. S.; Hu, L. B., Porous Amorphous FePO4 Nanoparticles Connected by Single-Wall Carbon Nanotubes for Sodium Ion Battery Cathodes. *Nano Lett* **2012,** 12, (11), 5664-5668.
13. Sathiya, M.; Hemalatha, K.; Ramesha, K.; Tarascon, J. M.; Prakash, A. S., Synthesis, Structure, and Electrochemical Properties of the Layered Sodium Insertion Cathode Material: NaNi1/3Mn1/3Co1/3O2. *Chem Mater* **2012,** 24, (10), 1846-1853.
14. Yabuuchi, N.; Kajiyama, M.; Iwatate, J.; Nishikawa, H.; Hitomi, S.; Okuyama, R.; Usui, R.; Yamada, Y.; Komaba, S., P2-type Na-x[Fe1/2Mn1/2]O-2 made from earth-abundant elements for rechargeable Na batteries. *Nat Mater* **2012,** 11, (6), 512-517.
15. Zhao, L.; Pan, H. L.; Hu, Y. S.; Li, H.; Chen, L. Q., Spinel lithium titanate (Li4Ti5O12) as novel anode material for room-temperature sodium-ion battery. *Chin. Phys .B* **2012,** 21, (2) 028201.

16. Zhao, L.; Zhao, J. M.; Hu, Y. S.; Li, H.; Zhou, Z. B.; Armand, M.; Chen, L. Q., Disodium Terephthalate (Na2C8H4O4) as High Performance Anode Material for Low-Cost Room-Temperature Sodium-Ion Battery. *Adv Energy Mater* **2012,** 2, (8), 962-965.

17. Thorne, J. S.; Dunlap, R. A.; Obrovac, M. N., Structure and Electrochemistry of NaxFexMn1-xO2 (1.0 <= x <= 0.5) for Na-Ion Battery Positive Electrodes. *J Electrochem Soc* **2013,** 160, (2), A361-A367.

18. Wang, L.; Lu, Y. H.; Liu, J.; Xu, M. W.; Cheng, J. G.; Zhang, D. W.; Goodenough, J. B., A Superior Low-Cost Cathode for a Na-Ion Battery. *Angew Chem Int Edit* **2013,** 52, (7), 1964-1967.

19. Yuan, D. D.; Hu, X. H.; Qian, J. F.; Pei, F.; Wu, F. Y.; Mao, R. J.; Ai, X. P.; Yang, H. X.; Cao, Y. L., P2-type Na0.67Mn0.65Fe0.2Ni0.15O2 Cathode Material with High-capacity for Sodium-ion Battery. *Electrochim Acta* **2014,** 116, 300-305.

20. Jian, Z. L.; Zhao, L.; Pan, H. L.; Hu, Y. S.; Li, H.; Chen, W.; Chen, L. Q., Carbon coated Na3V2(PO4)(3) as novel electrode material for sodium ion batteries. *Electrochem Commun* **2012,** 14, (1), 86-89.

21. Yu, X. Q.; Pan, H. L.; Wan, W.; Ma, C.; Bai, J. M.; Meng, Q. P.; Ehrlich, S. N.; Hu, Y. S.; Yang, X. Q., A Size-Dependent Sodium Storage Mechanism in L(i)4Ti(5)O(12) Investigated by,a Novel Characterization Technique Combining in Situ X-ray Diffraction and Chemical Sodiation. *Nano Lett* **2013,** 13, (10), 4721-4727.

22. Wang, Y. S.; Yu, X. Q.; Xu, S. Y.; Bai, J. M.; Xiao, R. J.; Hu, Y. S.; Li, H.; Yang, X. Q.; Chen, L. Q.; Huang, X. J., A zero-strain layered metal oxide as the negative electrode for long-life sodium-ion batteries (vol 4, 2365, 2013). *Nat Commun* **2013,** 4, 2365.

23. Delmas, C.; Fouassier, C.; Hagenmuller, P., Structural Classification and Properties of the Layered Oxides. *Physica B & C* **1980,** 99, (1-4), 81-85.

24. Mendiboure, A.; Delmas, C.; Hagenmuller, P., New Layered Structure Obtained by Electrochemical Deintercalation of the Metastable Lico02 (02) Variety. *Mater Res Bull* **1984,** 19, (10), 1383-1392.

25. Berthelot, R.; Carlier, D.; Delmas, C., Electrochemical investigation of the P2-NaxCoO2 phase diagram. *Nat Mater* **2011,** 10, (1), 74-U3.

26. Armstrong, A. R.; Lyness, C.; Panchmatia, P. M.; Islam, M. S.; Bruce, P. G., The lithium intercalation process in the low-voltage lithium battery anode Li1+xV1-xO2. *Nat Mater* **2011,** 10, (3), 223-229.

27. Braconnier, J. J.; Delmas, C.; Fouassier, C.; Hagenmuller, P., Electrochemical Behavior of the Phases Naxcoo2. *Mater Res Bull* **1980,** 15, (12), 1797-1804.

28. Delmas, C.; Braconnier, J. J.; Fouassier, C.; Hagenmuller, P., Electrochemical Intercalation of Sodium in Naxcoo2 Bronzes. *Solid State Ionics* **1981,** 3-4, (Aug), 165-169.

29. Shacklette, L. W.; Jow, T. R., Rechargeable Electrodes from Sodium Cobalt Bronzes. *J Electrochem Soc* **1987,** 134, (8B), C406-C406.

30. Molenda, J.; Delmas, C.; Hagenmuller, P., Electronic and Electrochemical Properties of Naxcoo2-Y Cathode. *Solid State Ionics* **1983,** 9-10, (Dec), 431-435.

31. Viciu, L.; Bos, J. W. G.; Zandbergen, H. W.; Huang, Q.; Foo, M. L.; Ishiwata, S.; Ramirez, A. P.; Lee, M.; Ong, N. P.; Cava, R. J., Crystal structure and elementary properties of NaxCoO2 (x=0.32, 0.51, 0.6, 0.75, and 0.92) in the three-layer NaCoO2 family. *Phys Rev B* **2006,** 73, (17).

32. Shu, G. J.; Chou, F. C., Sodium-ion diffusion and ordering in single-crystal P2-Na(x)CoO(2). *Phys Rev B* **2008,** 78, (5).

33. Lu, X.; Sun, Y.; Jian, Z. L.; He, X. Q.; Gu, L.; Hu, Y. S.; Li, H.; Wang, Z. X.; Chen, W.; Duan, X. F.; Chen, L. Q.; Maier, J.; Tsukimoto, S.; Ikuhara, Y., New Insight into the Atomic Structure of Electrochemically Delithiated O3-Li(1-x)CoO2 (0 <= x <= 0.5) Nanoparticles. *Nano Lett* **2012,** 12, (12), 6192-6197.

34. Reimers, J. N.; Dahn, J. R., Electrochemical and Insitu X-Ray-Diffraction Studies of Lithium Intercalation in Lixcoo2. *J Electrochem Soc* **1992,** 139, (8), 2091-2097.

35. Amatucci, G. G.; Tarascon, J. M.; Klein, L. C., CoO2, the end member of the LixCoO2 solid solution. *J Electrochem Soc* **1996,** 143, (3), 1114-1123.

36. Van der Ven, A.; Aydinol, M. K.; Ceder, G.; Kresse, G.; Hafner, J., First-principles investigation of phase stability in Li(x)CoO(2). *Phys Rev B* **1998,** 58, (6), 2975-2987.

37. Gu, L.; Zhu, C. B.; Li, H.; Yu, Y.; Li, C. L.; Tsukimoto, S.; Maier, J.; Ikuhara, Y., Direct Observation of Lithium Staging in Partially Delithiated LiFePO4 at Atomic Resolution. *J Am Chem Soc* **2011,** 133, (13), 4661-4663.

38. Lu, X.; Zhao, L.; He, X. Q.; Xiao, R. J.; Gu, L.; Hu, Y. S.; Li, H.; Wang, Z. X.; Duan, X. F.; Chen, L. Q.; Maier, J.; Ikuhara, Y., Lithium Storage in Li4Ti5O12 Spinel: The Full Static Picture from Electron Microscopy. *Adv Mater* **2012,** 24, (24), 3233-3238.

39. Lu, X.; Jian, Z. L.; Fang, Z.; Gu, L.; Hu, Y. S.; Chen, W.; Wang, Z. X.; Chen, L. Q., Atomic-scale investigation on lithium storage mechanism in TiNb2O7. *Energ Environ Sci* **2011,** 4, (8), 2638-2644.

40. Sun, Y.; Zhao, L.; Pan, H. L.; Lu, X.; Gu, L.; Hu, Y. S.; Li, H.; Armand, M.; Ikuhara, Y.; Chen, L. Q.; Huang, X. J., Direct atomic-scale confirmation of three-phase storage mechanism in Li4Ti5O12 anodes for room-temperature sodium-ion batteries. *Nat Commun* **2013,** 4, 1870.

41. He, X. Q.; Gu, L.; Zhu, C. B.; Yu, Y.; Li, C. L.; Hu, Y. S.; Li, H.; Tsukimoto, S.; Maier, J.; Ikuhara, Y.; Duan, X. F., Direct Imaging of Lithium Ions Using Aberration-Corrected Annular-Bright-Field Scanning Transmission Electron Microscopy and Associated Contrast Mechanisms. *Mater Express* **2011,** 1, (1), 43-50.

42. Suo, L. M.; Han, W. Z.; Lu, X.; Gu, L.; Hu, Y. S.; Li, H.; Chen, D. F.; Chen, L. Q.; Tsukimoto, S.; Ikuhara, Y., Highly ordered staging structural interface between LiFePO4 and FePO4. *Phys Chem Chem Phys* **2012,** 14, (16), 5363-5367.

43. Jian, Z.; Yuan, C.; Han, W.; Lu, X.; Gu, L.; Xi, X.; Hu, Y.-S.; Li, H.; Chen, W.; Chen, D.; Ikuhara, Y.; Chen, L. Q., Atomic Structure and Kinetics of NASICON NaxV2(PO4)3 Cathode for Sodium-Ion Batteries. *Adv. Funct. Mater.* **2014**, 10.1002/adfm.201400173.

44. Findlay, S. D.; Shibata, N.; Sawada, H.; Okunishi, E.; Kondo, Y.; Yamamoto, T.; Ikuhara, Y., Robust atomic resolution imaging of light elements using scanning transmission electron microscopy. *Appl Phys Lett* **2009,** 95, (19).

45. Findlay, S. D.; Shibata, N.; Sawada, H.; Okunishi, E.; Kondo, Y.; Ikuhara, Y., Dynamics of annular bright field imaging in scanning transmission electron microscopy. *Ultramicroscopy* **2010,** 110, (7), 903-923.